Optics and Lasers in Engineering 141 (2021) 106557

Contents lists available at ScienceDirect

Optics and Lasers in Engineering

journal homepage: www.elsevier.com/locate/optlaseng

Measuring two vibrations using dual-external-cavity structure in a self-mixing system ☆

Xiangyu Cui [b], Yuwei Liu [c], Peng Chen [a,*], Chunsheng Li [b,*]

[a] College of Electrical and Information Engineering, Northeast Petroleum University, Daqing 163318, China
[b] College of Computer and Information Technology, Northeast Petroleum University, Daqing 163318, China
[c] School of Instrumentation and Optoelectronic Engineering, Beihang University, Beijing 100191, China

ARTICLE INFO

Keywords:
Dual-external-cavity structure
self-mixing interference
measurement two vibrations simultaneously

ABSTRACT

This paper introduces a new dual-external-cavity structure in self-mixing interference system to be used with a semiconductor laser, and develops an improved algorithm for dominant and secondary harmonic order determination based on Fourier transform. The simulation and experimental results demonstrate that the proposed system can measure two vibrations simultaneously by using only a single detector and a single laser.

1个PD 1个LD实现2个振动测量

http://dx.doi.org/10.1364/OL.99.099999

1. Introduction

The output powers and frequencies of lasers can be altered by the feedback effect of the reflected light, which is portion of the output light that is reflected by the external cavity into the inner active cavity of the laser. The underlying phenomenon is self-mixing interference (SMI), which has been widely examined and applied in measuring several parameters, including distance [1], displacement [2,3], velocity [4,5], and vibration [6-8] because of its inherent simplicity [9], compactness [10,11], and self-alignment capability [12,13].

Several papers have examined the dual-channel SMI in fiber lasers. According to Wang et al. [14-16], applying SMI to parallel dual-channel fiber ring lasers can efficiently measure multiple displacements and velocities, although this approach does require use of two photodetectors (PDs) to measure two objects. Lu et al. [17] used the linear cavity of a fiber laser with a dual-channel SMI to measure vibrations, but this method required the use of an orthogonal Michelson interferometer in combination with a phase generated carrier demodulation method to demodulate the vibration signals. Moreover, both of these studies have employed complex devices and algorithms, thereby increasing the complexity and cost of the fiber laser structure with dual-channel SMI.

The SMI technique is intrinsically more efficient when using a class B laser (e.g., semiconductor laser) [17]. Nevertheless, semiconductor lasers with a dual-channel SMI are rarely used in measuring the multi-dimensional information of an object or the similar information of two objects.

This study proposed a new dual-external-cavity SMI structure for semiconductor lasers that can measure two vibrations with only a single detector and a single laser. To recover the vibrations from modulated SMI signals, this study also introduces an improved algorithm for dominant and secondary harmonic order determination based on Fourier transform (FT). Compared with the algorithm for dominant harmonic order determination proposed by Huang [18], the proposed improved algorithm can provide robust estimations of the vibration frequencies and amplitudes of two objects simultaneously.

2. Theoretical analysis

谐波阶数确定的改进算法，同时对两个物体的振动频率和振幅进行鲁棒性估计

2.1. A. SMI structures with a single cavity

The conventional single external cavity self-mixing model [19] is shown in Fig. 1, where r_1 and r_2 denote the reflection coefficients of laser facets R_1 and R_2, respectively, L_D denotes the length of the laser active cavity, L denotes the length of the external cavity (calculated as the distance from R_2 to the target M), and ΔL denotes the movement distance of the target M. A PD is typically used to detect any changes in power.

2.2. B. Amplitude and frequency solution for SMI with a single cavity

The output power detected by the PD can be expressed as follows [20]:

$$P = P_0[1 + m\cos(\omega \cdot \tau(t))] \quad (1)$$

where P and P_0 are the light intensities with and without feedback, respectively, and m is the modulation index that reflects the visibility

☆ Received XX Month XXXX; revised XX Month, XXXX; accepted XX Month XXXX; posted XX Month XXXX (Doc. ID XXXXX); published XX Month XXXX
* Corresponding author.
E-mail addresses: eq0687@126.com (P. Chen), csli0886@163.com (C. Li).

https://doi.org/10.1016/j.optlaseng.2021.106557
Received 29 September 2020; Received in revised form 30 December 2020; Accepted 22 January 2021
Available online 4 February 2021

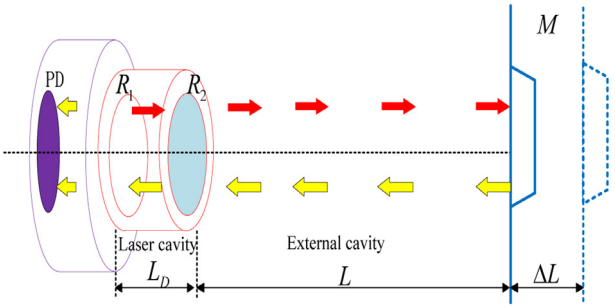

Fig. 1. Structure of the three-cavity F–P model for SMI.

of the interference fringes. A higher $m$corresponds to a higher signal-to-noise ratio for the interference signal. Here, $\omega = 2\pi\nu$ is the angular frequency of the laser, where ν denotes the optical frequency of the laser, $\tau = 2L/c$ is the round trip time of the laser beam in the external cavity, and c denotes the speed of light.

The laser wavelength is no longer the initial wavelength λ_0 but becomes equal to λ because of the optical feedback modulation. The change in wavelength is determined by solving the following phase equation:

$$\omega_0\tau = \omega\tau + C\sin(\omega\tau + \arctan\alpha) \tag{2}$$

where $\omega_0 = 2\pi\nu_0$ is the angular frequency without feedback, ν_0 denotes the optical frequency of the laser without feedback, C is an optical feedback parameter, and α is the linewidth broadening factor. $\omega_0\tau$ and $\omega\tau$ denote the phases without and with optical feedback, respectively.

By combining Eq. (1) and (2), the laser output power can be formulated as follows:

$$P = P_0\{1 + m\cos[\varphi + a\sin(2\pi f_0 t + \phi)]\} \tag{3}$$

where f_0 is the vibration frequency, ϕ is the initial phase, and t is the time variable

$$\varphi = 4\pi L/\lambda \tag{4}$$

$$a = 4\pi A/\lambda \tag{5}$$

By expanding the normalized laser output power in a trigonometric series, we obtain the following:

$$\begin{aligned}\Delta P &= \cos\varphi J_0(a)\\ &+ \cos\varphi e^{j2n\phi}\sum_{n=1}^{\infty} J_{2n}(a)e^{j2n\cdot 2\pi f_0 t}\\ &+ \cos\varphi e^{-j2n\phi}\sum_{n=1}^{\infty} J_{2n}(a)e^{-j2n\cdot 2\pi f_0 t}\\ &- j\sin\varphi e^{j(2n+1)\phi}\sum_{n=0}^{\infty} J_{2n+1}(a)e^{j(2n+1)\cdot 2\pi f_0 t}\\ &- j\sin\varphi e^{-j(2n+1)\phi}\sum_{n=0}^{\infty} J_{2n+1}(a)e^{-j(2n+1)\cdot 2\pi f_0 t}\end{aligned} \tag{6}$$

where $J_{2n}(a)$ and $J_{2n+1}(a)$ are even- and odd-order Bessel functions of the first kind with argument a, respectively. The independent variable n is a positive integer. When only the direct-current (DC) and positive components of the frequency are considered, the FT model of Eq. (11) can be written as follows:

$$\begin{aligned}|F(f)| &= \cos\varphi|J_0(a)|\delta(f)\\ &+ \cos\varphi\sum_{n=1}^{\infty}|J_{2n}(a)|\delta(f - 2nf_0)\\ &+ \sin\varphi\sum_{n=0}^{\infty}|J_{2n+1}(a)|\delta[f - (2n-1)f_0]\end{aligned} \tag{7}$$

where $\delta(f)$ is the impulse function, and f is the frequency. In Eq. (7), $|F(f)|$ comprises f_0 and its harmonic components. When $J_n(a)$ reaches the maximum, the nth-order harmonic component is regarded as the maximum. n is then marked as n_d. The n_dth-order harmonic component

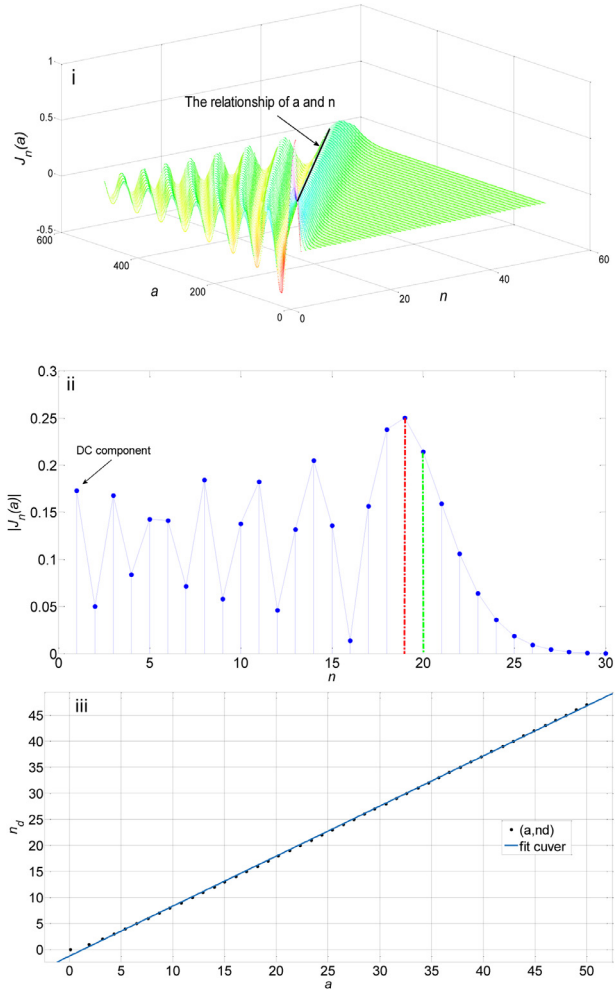

Fig. 2. Principle of the dominant harmonic order. (i) The Bessel function of the first kind that varies along with n and a; (ii) the relationship between $|J_n(a)|$ and n, n_d (iii) the relationship between a and n_d.

is equivalent to the maximum frequency in the spectrum and is called the dominant harmonic order. By using the fast Fourier transform(FFT), the frequency of the vibration can be acquired easily but the amplitude can't be measured, so this paper further studied in order to measure vibration.

The value of the Bessel function with changing n and a is shown in Fig. 2(i). For a specific$a$, $J_n(a)$ changes along with n. The relationship between $|J_n(a)|$ and n when $a = 20$ is illustrated in Fig. 2(ii).

From Fig. 2(ii). it's clear that when a is a fixed value,$J_n(a)$ has several maxima and one maxima in the range.

Record the corresponding n when $J_n(a)$ is the maximum value as n_d. In the laser self-mixing interference spectrum generated by the vibrating object, the frequency corresponding to n_d is recorded as f_{n_d} which is considered the main frequency, and record the frequency corresponding to $n_d + 1$ as f_{n_d+1}.

As shown in Fig. 2(iii), the following relationship between n_d and a can be obtained after fitting:

$$n_d = 0.96a - 1.25 \tag{8}$$

By substituting Eq. (8) into Eq. (5) and by assuming that$\lambda \approx \lambda_0$, the following equation can be derived:

$$A = \frac{n_d + 1.25}{0.96}\frac{\lambda_0}{4\pi} \tag{9}$$

f_0 should be obtained afterward. In previous studies [18, 21], f_0 was obtained on the basis that its value is equal to the fundamental frequency.

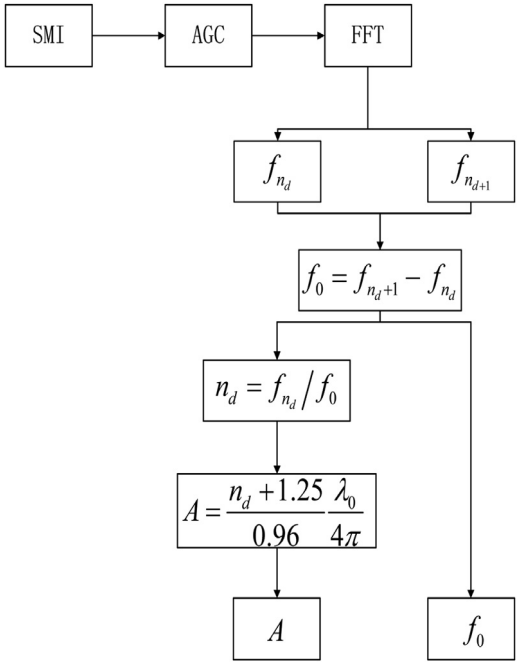

Fig. 3. Principle of the dominant and secondary harmonic order determination.

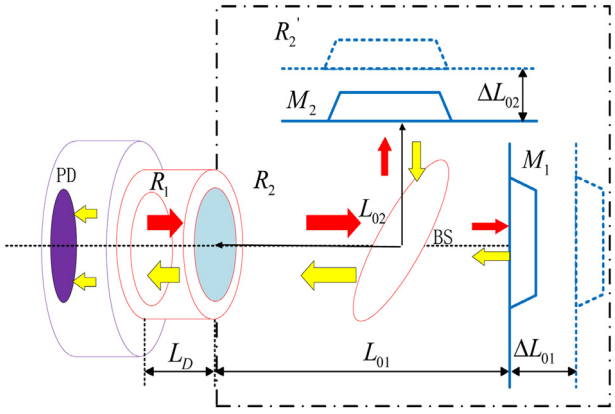

Fig. 4. Laser SMI structure with dual-external cavities.

However, in reality, the basic frequency may be submerged within the noise or spectrum of another frequency when the two signals are mixed. In such a case, f_0 cannot be calculated accurately. To solve this problem, f_0 is calculated by using Eq. (10), where the frequency of n_d is denoted by f_{n_d}, while the frequency of $n_d + 1$ is denoted by f_{n_d+1}:

$$f_0 = (n_d + 1) f_0 - n_d f_0 = f_{n_d+1} - f_{n_d} \tag{10}$$

where f_{n_d} and f_{n_d+1} can be found within the SMI spectrum.

Thus, the improved vibration measurement algorithm called dominant and secondary harmonic order determination is illustrated in Fig. 3.

The condition $\varphi = K\pi/2, K = 1, 2, 3 \ldots$ must be avoided during the operation because the amplitude of the basic frequency or the odd harmonic components in this case is 0. The initial phase φ can be varied by adjusting L (initial length).

2.3. C. SMI structures with a dual-external-cavity

In order to measure two vibrations simultaneously by using only a single detector and a single laser, SMI structures with a dual-external-cavity is proposed in this paper. The optical path obtained by using dual external cavities when SMI occurs is depicted in Fig. 4. A portion of the light from the laser cavity passes through R_2 and then travels toward the beam splitter (BS). Afterward, one part of the light travels toward the moving target M_1, while the another part travels toward the moving target M_2. The light reflected by M_1 and M_2 is subsequently transmitted through both BS and R_2 before returning to the laser cavity. Here, t_2 is the transmittance of R_2, r_3 and r_4 are the reflectivity values of M_1 and M_2, respectively, L_{01} is the length of external cavity 1 (from R_2 to M_1), and L_{02} is the length of external cavity 2 (from R_2 to M_2). In addition, ΔL_{01} and ΔL_{02} are the movement distances of targets M_1 and M_2, respectively, while t_{BS} and r_{BS} are the transmittance and reflectance of the BS, respectively. We let R_2 and the dual-external-cavity structure be equivalent to R_2'. The equivalent reflectance under the weak feedback condition $\eta \le 1$ can be written as follows:

$$\ln(|r_2'|) \approx \ln r_2 + \eta t_2^2 \left[t_{BS}^2 r_3 \cos\alpha_1 + r_{BS}^2 r_4 \cos\alpha_2 \right] \tag{11}$$

$$\begin{aligned} \alpha &= \arctan \frac{\eta t_2^2 \left[t_{BS}^2 r_3 \sin\alpha_1 + r_{BS}^2 r_4 \sin\alpha_2 \right]}{r_2 + \eta t_2^2 \left[t_{BS}^2 r_3 \cos\alpha_1 + r_{BS}^2 r_4 \cos\alpha_2 \right]} \\ &\approx \eta t_2^2 / r_2 \left[t_{BS}^2 r_3 \sin\alpha_1 + r_{BS}^2 r_4 \sin\alpha_2 \right] \end{aligned} \tag{12}$$

where η is the coupling coefficient of the feedback light, $\alpha_1 = 2kL_{01}$ is the phase of external cavity 1, and $\alpha_2 = 2kL_{02}$ is the phase of external cavity 2.

The threshold condition of the dual-external-cavity structure can be described as:

$$r_1 r_2' \exp(2gkL_D) \exp(i2n_c kL_D + i\alpha) = 1 \tag{13}$$

$$\begin{cases} gk = -\frac{1}{2L_D} \ln\left(r_1 |r_2'|\right) \\ 2nkL_D + \alpha = 2m\pi \end{cases} \tag{14}$$

From the F–P laser cavity, the power equation can be deduced as follows:

$$\omega_0 \tau_D = \omega\tau_D - \left[C_1 \sin(\omega\tau_1) + C_2 \sin(\omega\tau_2) \right] \tag{15}$$

$$P = P_0(1 - K\Delta G) = P_0\left[1 - \mu_1 \cos(\omega\tau_1) - \mu_2 \cos(\omega\tau_2) \right] \tag{16}$$

where $\tau_D = 2n_0 L_D / c$ (in which τ_D is the round trip time of the laser beam in the laser cavity, and c is the speed of light), $\tau_1 = 2L_{01}/c$ (in which τ_1 is the round trip time of the laser beam in external cavity 1), and $\tau_2 = 2L_{02}/c$ (in which τ_2 is the round trip time of the laser beam in external cavity 2). In addition, $C_1 = \eta t_{BS}^2 r_3 t_2^2 / r_2$ and $C_2 = \eta r_{BS}^2 r_4 t_2^2 / r_2$ are the external feedback strength parameters, K is the laser cavity constant, P_0 is the initial light intensity without feedback, and $\mu_1 = \eta t_{BS}^2 r_3 t_2^2$ and $\mu_2 = \eta r_{BS}^2 r_4 t_2^2$ are the undulation coefficients of SMI.

Equations (15) and (16) indicate that using the SMI with a dual-external-cavity structure is equivalent to using two SMI systems and can therefore be applied in a multichannel measurement environment.

2.4. D. Solutions for the amplitudes and frequencies in SMI with a dual-external-cavity structure

Similar to Fig. 4, L_{01} represents the initial distance between R_2 and M_1, while L_{02} represents the initial distance between R_2 and M_2. Assuming that both M_1 and M_2 perform simple harmonic vibrations, the motions of the dual external cavities can be given as follows:

$$L_{01}(t) = L_{01} + \Delta L_{01} = L_{01} + A_1 \sin(2\pi f_1 t + \varphi_1) \tag{17}$$

$$L_{02}(t) = L_{02} + \Delta L_{02} = L_{02} + A_2 \sin(2\pi f_2 t + \varphi_2) \tag{18}$$

where A_1 and A_2 are the vibration amplitudes of M_1 and M_2, respectively, f_1 and f_2 are the frequencies of the two vibrations, and φ_1 and φ_2 are the initial phases of M_1 and M_2, respectively.

By combining Eqs. (16), (17), and (18), the laser output power can be written as follows:

$$P = P_0\left[1 - \mu_1 \cos(\psi_{01} + a_1 \sin(2\pi f_1 t + \varphi_1)) - \mu_2 \cos(\psi_{02} + a_2 \sin(2\pi f_2 t + \varphi_2)) \right]$$

m

(19)

where

$$\psi_{01} = \frac{4\pi L_{01}}{\lambda} \tag{20}$$

lambdaF

$$\psi_{02} = \frac{4\pi L_{02}}{\lambda} \tag{21}$$

$$a_1 = \frac{4\pi A_1}{\lambda} \tag{22}$$

$$a_2 = \frac{4\pi A_2}{\lambda} \tag{23}$$

Similarly, the expansion of the normalized laser output power in a trigonometric series can be written as follows:

$$\Delta P(t) = \begin{bmatrix} \mu_1 \cos\psi_{01} J_0(a_1) \\ +\mu_1 \cos\psi_{01} \sum_{m=1}^{\infty} J_{2m}(a_1) e^{j2m\varphi_{01}} \\ +\mu_1 \cos\psi_{01} \sum_{m=1}^{\infty} J_{2m}(a_1) e^{-j2m\varphi_{01}} \\ +j\mu_1 \sin\psi_{01} \sum_{m=1}^{\infty} J_{2m-1}(a_1) e^{j2(m-1)\varphi_{01}} \\ -j\mu_1 \sin\psi_{01} \sum_{m=1}^{\infty} J_{2m-1}(a_1) e^{-j2(m-1)\varphi_{01}} \end{bmatrix} + \begin{bmatrix} \mu_2 \cos\psi_{02} J_0(a_2) \\ +\mu_2 \cos\psi_{02} \sum_{m=1}^{\infty} J_{2m}(a_2) e^{j2m\varphi_{02}} \\ +\mu_2 \cos\psi_{02} \sum_{m=1}^{\infty} J_{2m}(a_2) e^{-j2m\varphi_{02}} \\ +j\mu_2 \sin\psi_{02} \sum_{m=1}^{\infty} J_{2m-1}(a_2) e^{j2(m-1)\varphi_{02}} \\ -j\mu_2 \sin\psi_{02} \sum_{m=1}^{\infty} J_{2m-1}(a_2) e^{-j2(m-1)\varphi_{02}} \end{bmatrix} \tag{24}$$

where, $\varphi_{01} = 2\pi f_1 t$, and $J_{2m}(a_1)$ and $J_{2m-1}(a_1)$ are the even- and odd-order Bessel functions of the first kind with argument a_1. Similarly, $J_{2m}(a_2)$and $J_{2m-1}(a_2)$ are the corresponding Bessel functions with the argument a_2. The independent variables a_1, a_2, and m are all positive integers. By considering only the DC component and the positive component of the frequency, the residual $|F_{12}(f)|$ can be written as follows:

$$|F_{12}(f)| = \begin{bmatrix} \mu_1 cos\psi_{01} |J_0(a_1)| \delta(f) \\ +\mu_1 cos\psi_{01} \sum_{m=1}^{\infty} |J_{2m}(a_1)| \delta(f - 2mf_1) \\ +j\mu_1 sin\psi_{01} \sum_{m=1}^{\infty} |J_{2m-1}(a_1)| \delta(f - (2m-1)f_1) \end{bmatrix} + \begin{bmatrix} \mu_2 cos\psi_{02} |J_0(a_2)| \delta(f) \\ +\mu_2 cos\psi_{02} \sum_{m=1}^{\infty} |J_{2m}(a_2)| \delta(f - 2mf_2) \\ +j\mu_2 sin\psi_{02} \sum_{m=1}^{\infty} |J_{2m-1}(a_2)| \delta(f - (2m-1)f_2) \end{bmatrix} \tag{25}$$

where the frequency spectrum is composed of f_1, f_2, and their harmonic components. If the frequencies are not mixing of two vibrations, we can separate the two signals by filtering, and then measure the vibration of each signal, but when the frequencies are mixing, filtering is not effective, the signals cannot be separated clearly. Thus, this paper proposed an improved algorithm for dominant and secondary harmonic order determination based on FT to measure two vibrations using dual-external-cavity structure simultaneously.

For the target M_2, the frequency of n_{d_1} is denoted by $f_{n_{d_1}}$, while the frequency of $n_{d_1}+1$ is denoted by $f_{n_{d_1}+1}$. Meanwhile, for the target M_2, the frequency of n_{d_2} is denoted by $f_{n_{d_2}}$, while the frequency of $n_{d_2}+1$ is denoted by $f_{n_{d_2}+1}$. Equations (25) and (13) are then compared, and the first and second parts can be processed as follows by using the approach illustrated in Fig. 3:

$$f_1 = f_{n_{d_1}+1} - f_{n_{d_1}} \tag{26}$$

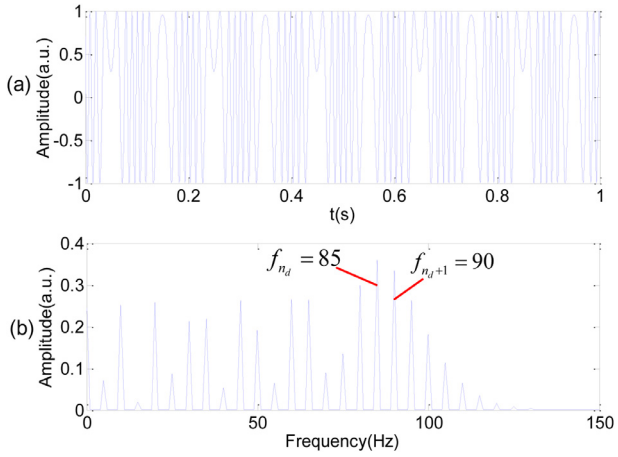

Fig. 5. Simulation results when $A = 1\mu m$ and $f_0 = 5Hz$. (a) SMI signals; and (b) frequency spectrum.

$$f_2 = f_{n_{d_2}+1} - f_{n_{d_2}} \tag{27}$$

$$A_1 = \frac{n_{d_1} + 1.25}{0.96} \frac{\lambda_0}{4\pi} \tag{28}$$

$$A_2 = \frac{n_{d_2} + 1.25}{0.96} \frac{\lambda_0}{4\pi} \tag{29}$$

3. Numerical simulation

仿真条件和结果

3.1. A. Simulation analysis of SMI with a single cavity

To analyze the practical aspects of the solutions for both amplitude and frequency in SMI when using a single cavity, as described in Section 2.2, we set the target to perform a sinusoidal motion with the amplitude of 1 μm and a frequency of 5 Hz. The sampling frequency is set to 32 kHz, while the number of sampling points is set to 32 K. Fig. 5.(a) and 5(b) show the simulated displacement and frequency spectrum of the target, respectively. When using the improved algorithm, the demodulated frequency is 5 Hz, while the demodulated amplitude is 0.984 μm.

3.2. B. Simulation analysis of SMI with a dual-external-cavity structure

To evaluate the feasibility of the proposed solution for the amplitudes and frequencies in SMI with a dual-external-cavity structure, as described in Section 2.3, we modulate $L_1(t)$ and $L_2(t)$ by using sinusoidal signals. These signals have frequencies of 2 Hz and 20 Hz, and have the same amplitude of 1 μm at $\lambda_0 = 650nm$. The simulated SMI signals are shown in Figs. 6(a) and 6(b), the simulated optical output power is illustrated in Fig. 6(c), and the frequency spectrum of the signal is shown in Fig. 6(d). The y axis of the four pictures is amplitude, the x axis of the first three pictures is time, the unit is second, and the abscissa of the last picture is frequency, the unit is hertz. In order to see the self-mixing interference fringes more intuitively, Fig. 5.2 (c) and Fig. 5.2 (d) respectively use the method shown in the figure to amplify the local signal.

正弦信号

According to the method of data processing in this article, we first find out $f_{n_{d_1}}$, $f_{n_{d_2}}$, $f_{n_{d_1}+1}$, $f_{n_{d_2}+1}$ in the FFT spectrum in Fig. 6(d). The $f_{n_{d_1}}$ of the spectrum is the marked point in the figure. The marked data's x axis is the coordinate of 34Hz, $f_{n_{d_1}+1}$ is the coordinate of the x axis of 36Hz; $f_{n_{d_2}}$ is the coordinate point of the x axis of 680Hz, and $f_{n_{d_1}+1}$ is the coordinate point of the x axis of 720Hz. The vibrations can be calculated by using the algorithm presented in Fig. 3. The demodulated

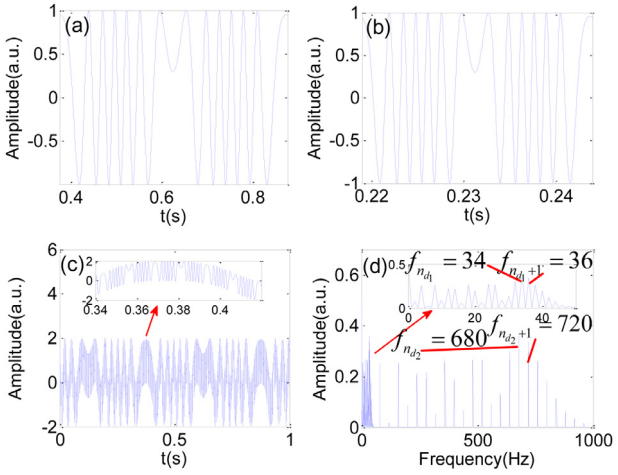

Fig. 6. Simulation results with $A_1 = 1\mu m$, $A_2 = 1\mu m$, $f_1 = 2Hz$, and $f_2 = 40Hz$. (a) SMI signal from external cavity 1, (b) SMI signal from external cavity 2, (c) SMI signal with a dual-external-cavity structure, and (d) frequency spectrum.

frequencies are 2 Hz and 40 Hz while the demodulated amplitude for both signals is 0.984 μm.

4. Experimental procedures and results

4.1. A. Experimental results for SMI with a single cavity

单腔实验

To further confirm the validity of this measurement solution, we set up an experimental bench as shown in Fig. 7. In this experimental setup, a laser diode (LD; QL65D5SA, QSI Co. Ltd., Korea) is packaged with a PD to detect its output power and an aspherical collimating lens and is driven by a constant current source (LD1255).

To ensure the accuracy of the results, we used a high-precision piezoelectric ceramic transducer (PZT; P753.1 CD, Physik Instrumente, Karlsruhe, Germany) as an external target. The resolution of this PZT can reach 0.05 nm when used in a closed-loop configuration. The current signal is converted into a voltage signal by using a transconductance amplifier, and the voltage signals are collected by using a data acquisition card (USB-4431, National Instruments Corp.) before being sent to a computer.

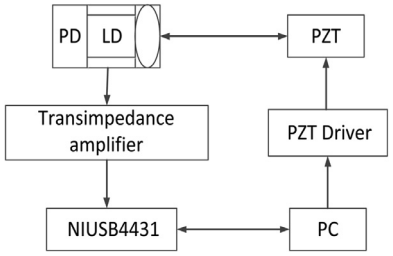

Fig. 7. Experimental setup for SMI with a single cavity.

A series of experiments was performed. First, the PZT was driven by using a sinusoidal waveform with a frequency of 5 Hz. Fig. 8(a) shows the SMI output signals with amplitudes of 1, 2, and 4 μm, while Fig. 8(b) shows the corresponding frequency spectra of these output signals. By using the method shown in Fig. 4, all demodulated frequencies were equal to 5 Hz, while their corresponding demodulated amplitudes were equal to 0.984, 2.008, and 4.002 μm, respectively.

Fig. 9(a) and (b) show the output signals and their corresponding frequency spectra for different PZT drive frequencies at a vibration amplitude of 1 μm. The PZT drive frequencies are set to 5, 10, and 20 Hz, which have corresponding demodulated frequencies of 5, 10, and 20 Hz as well as demodulated amplitudes of 0.984, 1.038, and 1.038 μm, respectively.

4.2. B. Experimental results for SMI with a dual-external-cavity structure

双外腔实验

The experimental setup for SMI with a dual-external-cavity structure is shown in Fig. 10. In addition to the setup shown in Fig. 7, a BS that divides the laser beam into two beams and a loudspeaker driven by a signal generator are included in this setup.

First, the PZT was driven by using a sinusoidal waveform with a frequency of 2 Hz and an amplitude of 1 μm, while the loudspeaker was driven by using a sinusoidal waveform with a frequency of 40 Hz and an amplitude of 1 μm. The SMI signal when using the dual-external-cavity structure is presented in Fig. 11(a), and the frequency spectrum that is determined by FT is shown in Fig. 11(b).

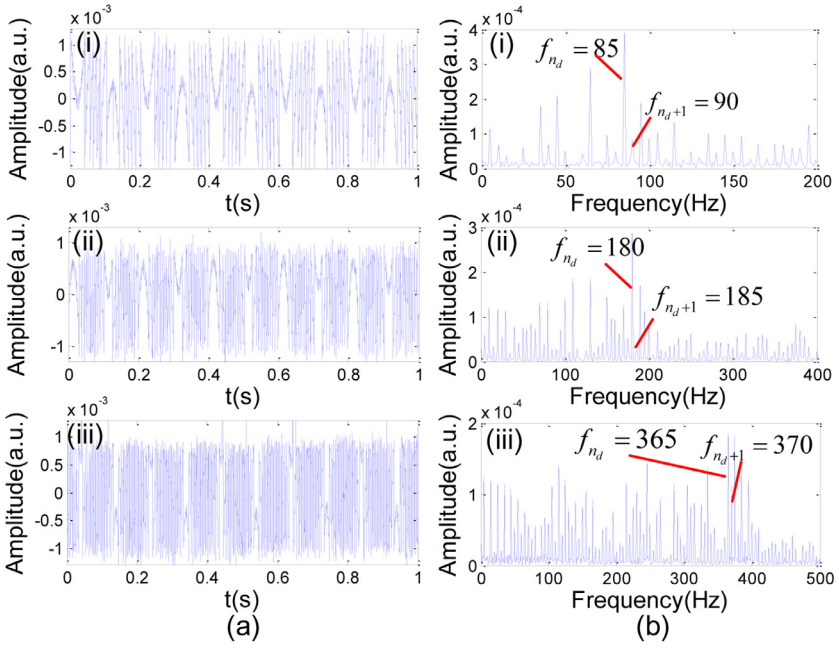

Fig. 8. Experimental results for SMI with a single cavity when $A = 1$, 2, and 4μm and $f_0 = 5Hz$. (a) SMI signals, and (b) frequency spectrum.

Table 1
Results of the three groups of experiments.

	Set				Measured				Error	
	PZT		Loudspeaker		PZT		Loudspeaker		PZT Loudspeaker	
	A_1	f_1	A_2	f_2	$\overline{A_1}$	$\overline{f_1}$	$\overline{A_2}$	$\overline{f_2}$	Error (A_1)	Error (A_2)
I	1	2	1	40	0.98	2	0.98	40	0.02	0.02
	2	2	1	40	1.95	2	0.98	40	0.05	0.02
	4	2	1	40	4.11	2	0.98	40	0.11	0.02
III	1	2	1	40	0.98	2	0.98	40	0.02	0.02
	1	2	2	40	1.04	2	2.01	40	0.04	0.01
	1	2	4	40	1.04	2	4	40	0.04	0.00
III	1	2	1	40	0.98	2	0.98	40	0.02	0.02
	1	2	1	60	0.98	2	0.98	60	0.02	0.02
	1	2	1	80	0.98	2	0.98	80	0.02	0.02

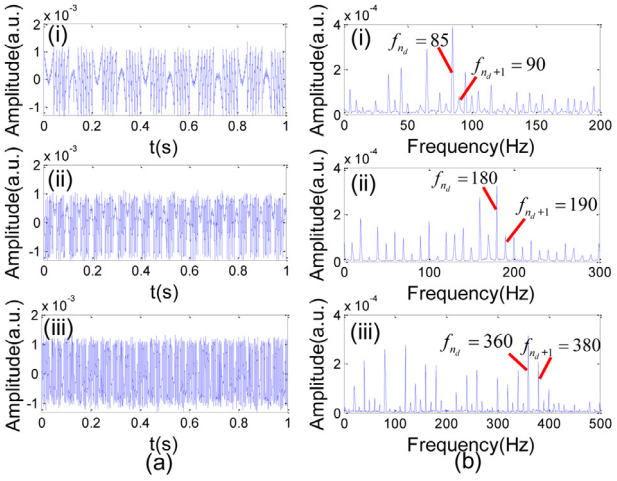

Fig. 9. Experimental results for SMI with a single cavity when $A = 1\mu m$ and $f_0 = 5$, 10, and 20 Hz. (a) SMI signals, and (b) frequency spectrum.

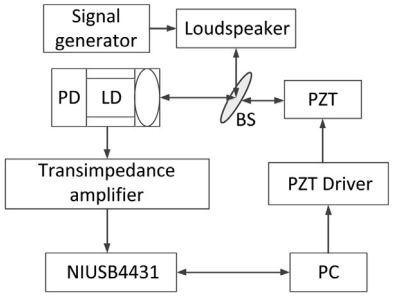

Fig. 10. Experimental setup for SMI with a dual-external-cavity structure.

As can be seen in Fig. 11(b), the demodulated frequencies are 2 Hz and 40 Hz, while the corresponding demodulated amplitudes are 0.984 μm and 0.984 μm, respectively.

Second, further experiments were conducted on a series of states. The vibration amplitude of the PZT was varied and its frequency was maintained at 2 Hz, while the loudspeaker was prevented from being driven by the signal with an amplitude of 1 μm and frequency of 40 Hz. The measurement results are listed in Table 1(I). The amplitude of the loudspeaker was then varied and its frequency was maintained at 40 Hz while the PZT was driven by an amplitude of 1 μm and frequency of 2 Hz. The measurement results are listed in Table 1(III). The PZT was then driven by an amplitude of 1 μm at frequency of 2 Hz, and the vibration frequency of the loudspeaker with a signal amplitude of 1 μm was driven invariably. The measurement results are listed in Table 1(III).

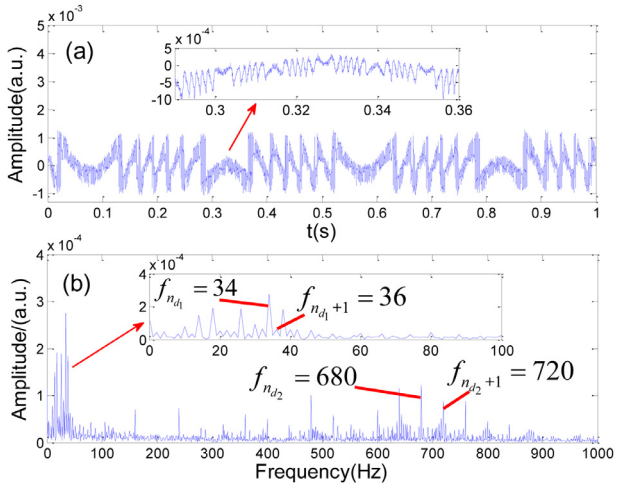

Fig. 11. Experimental results for SMI with a dual-external-cavity structure when, $A_1 = 1\mu m$, $A_2 = 1\mu m$, $f_1 = 2$Hz, and $f_2 = 40$Hz. (a) SMI signal, and (b) frequency spectrum.

The measured frequencies are consistent with the set frequencies, and the measured amplitudes show a favorable agreement with the set amplitudes. However, the measured amplitudes show slight errors that may be caused by numerical quantification and electronic noise [22].

5. Discussion

This paper uses a single laser to achieve dual-channel vibration measurement. In theory, when the frequency of the measured vibration is quite different, this method can be used to measure more than two targets, and is not limited to dual-channel measurement. In the measurement, the intervention of the speckle random signal will cause complicated interference in the time domain analysis. In this paper, by converting the time domain analysis into a simpler and more intuitive frequency domain analysis, it is more robust. This is because in the time domain analysis, due to the intervention of speckle random signals, there is too much interference in the time domain, which is very complicated. However, studying the frequency components of the signal in the frequency domain reduces the time complexity in the signal analysis and processing process, is more robust, and is less affected by the speckle signal.

In actual industrial production, this technology can be developed as a two-dimensional sensor, which has a wide range of application prospects, such as the detection of horizontal and vertical axis of pipeline leaks, the multi-directional simultaneous measurement of stones in the human body in medical field, and the detection of underground oil in oil and gas development sector.

6. Conclusions

In this study, a new SMI system with a dual-external-cavity structure is developed to be used with a semiconductor laser, and an improved algorithm for dominant and secondary harmonic order determination is proposed based on FT. A series of simulations and experiments were also performed to verify the feasibility of the proposed structure and the effectiveness of the algorithm. The results of these simulations and experiments demonstrated that the algorithm could measure two vibrations robustly by using only a single detector and a single laser.

Declaration of Competing Interest

The authors declared that they have no conflicts of interest to this work. We declare that we do not have any commercial or associative interest that represents a conflict of interest in connection with the work submitted.

CRediT authorship contribution statement

Xiangyu Cui: Conceptualization, Methodology, Software, Data curation, Writing - original draft. **Yuwei Liu:** Software, Validation. **Peng Chen:** Supervision. **Chunsheng Li:** Visualization, Investigation, Writing - review & editing.

Funding

The Innovation Project of Postgraduate Education of in Northeast Petroleum University (JYCX_CX06_2018, JYCX_JG06_2018).

References

[1] Kou Ke, Li Xingfei, Li Li, Xiang Hongbiao. Injected current reshaping in distance measurement by laser self-mixing interferometry. Appl. Optics 2014;53(27):6280–6.
[2] Huang Z. Piece-wise transition detection algorithm for a self-mixing displacement sensor. Chin. Opt. Lett 2013;11(9):8–12.
[3] Wang M, Lai GM. Displacement measurement based on Fourier transform method with external laser cavity modulation. Review of Scientific Instruments 2001;72(8):3440–5.
[4] Gao Bingkun, Qing Chen, Yin Shunxin, Peng Chen, Jiang Chunlei. Measurement of rotation speed based on double-beam self-mixing speckle interference. Opt. Lett 2018;43(7):1531–3.
[5] Du Z, Lu L, Zhang W, Yang B, Gui H, Yu B. Measurement of the velocity inside an all-fiber dbr laser by self-mixing technique. Applied Physics B 2013;113(1):153–8.
[6] Magnani Alessandro, Pesatori Alessandro, Norgia Michele. Self-mixing vibrometer with real-time digital signal elaboration. Appl. Optics 2012;51(21):5318–25.
[7] Lu L, Zhai L, Zhang K, Dai J, Zhu J, Zhen S. The study of laser self-mixing vibrometer employing different feedback regime using a vcsels. Optik - International Journal for Light and Electron Optics 2011;122(20):1840–2.
[8] Yu B, Yang J, Liang L, Zhai L, Wang R, Cao Z. Self-mixing interference measurement system of a fiber ring laser with ultra-narrow linewidth. Opt. Express 2012;20(8):8598.
[9] Bernal OD, Zabit U, Bosch TM. Robust method of stabilization of optical feedback regime by using adaptive optics for a self-mixing micro-interferometer laser displacement sensor. IEEE J Sel Top Quant 2015;21(4).
[10] Sudo S, Otsuka K. Measurements of liquid surface fluctuations using a self-mixing solid-state laser. Journal of Applied Physics 2014(23):115.
[11] Dmitriev AK, Konovalov AN, Ul'yanov VA. Self-mixing detection of backscattered radiation in a single-mode erbium fibre laser for Doppler spectroscopy and velocity measurements. Quantum Electronics 2014;44(4):309–13.
[12] Lu L, Cao ZG, Dai JJ, Xu F, Yu BL. Self-Mixing Signal in Er3+-Yb3+ Codoped Distributed Bragg Reflector Fiber Laser for Remote Sensing Applications up to 20 Km. IEEE Photonic Tech L 2012;24(5):392–4.
[13] Guo DM, Wang M. Self-mixing interferometry based on a double-modulation technique for absolute distance measurement. Appl. Optics 2007;46(9):1486–91.
[14] Wang M, Dai X, Zhou J, Han D, Zhao Y. Self-mixing interference in fiber lasers and its applications. In: Proc. SPIE, 7544; 2010.
[15] Wang M, Xia W, Zhao Y, Han D. Self-mixing interference in fiber ring laser: Application for displacement and velocity measurement. Proc. SPIE 2012;8413 84131S-84131S-5.
[16] Zhao Y, Wang M, Zhou J, Dai X. Self-mixing interference in fiber ring laser with parallel dual-channel. IEEE Photonic Tech L 2009;21(13):863–5.
[17] Lu L, Zhang W, Yang B, Zhou J, Gui H, Yu B. Dual-channel self-mixing vibration measurement system in a linear cavity fiber laser. IEEE Sensors Journal 2013;13(11):4387–92.
[18] Huang Z, Sun X, Li C. Self-mixing interference signal analysis based on Fourier transform method for vibration measurement. Opt. Eng. 2013.
[19] Bosch TM, Servagent N, Gouaux F, Mourat G. Self-mixing interference inside a laser diode: Application for displacement, velocity, and distance measurement. Proc. SPIE 1998;3478:98–108.
[20] Roths J, Breinbauer M, Hilber B, Gerz C, Koltchanov I, Petermann K. Interferometric displacement measurements performed with a self-mixing micro-interferometer. Proc. SPIE 1997;3098:411–21.
[21] Dai X, Wang M, Zhao Y, Zhou J. Self-mixing interference in fiber ring laser and its application for vibration measurement. Opt. Express 2009;17(19):16543.
[22] Wang X, Guo X, Wang Y, et al. All-fiber differential interferometer for nanometric displacement measurement[J]. Optics Communications 2020;475:126283.